Journal of the European Ceramic Society 40 (2020) 78–84

Contents lists available at ScienceDirect

Journal of the European Ceramic Society

journal homepage: www.elsevier.com/locate/jeurceramsoc

Original Article

Densification, morphological and transport properties of functional $La_{1-x}Ba_xYbO_{3-\delta}$ ceramic materials

Anna V. Kasyanova[a,b], Julia G. Lyagaeva[a,b,*], Andrey S. Farlenkov[a,b], Alexey I. Vylkov[a,b], Sergey V. Plaksin[a], Dmitry A. Medvedev[a,b,*], Anatoly K. Demin[a,b]

[a] Institute of High Temperature Electrochemistry, 620137, Yekaterinburg, Russia
[b] Ural Federal University, 620002, Yekaterinburg, Russia

ARTICLE INFO

Keywords:
$LaYbO_3$
Perovskite
CO_2-tolerance
Transport properties
Proton-conducting electrolytes

ABSTRACT

The effective operation of protonic ceramic electrochemical cells requires the design of electrolytes having not only high ionic conductivity, but also excellent stability with respect to carbonisation. In the present work, the La-based oxides ($La_{1-x}Ba_xYbO_{3-}\delta$, $0.03 \le x \le 0.10$) are proposed as a possible alternative to the convenient Ba(Ce,Zr)O_3-based electrolytes due to their high chemical stability. It was discovered that Ba-doping results in a deterioration of sintering behaviour; as a result, the relative density decreases and open porosity appears (for $x = 0.10$). A thorough analysis of transport properties by means of AC and DC measurement techniques enables a selection of the $La_{0.97}Ba_{0.03}YbO_{3-}\delta$ sample, which demonstrates the highest conductivity compared with those samples where $x = 0.5$ and 0.10. Due to its excellent densification behaviour, stability and ionic conductivity, $La_{0.97}Ba_{0.03}YbO_{3-}\delta$ can be considered as a promising proton-conducting electrolyte in the La-based family.

1. Introduction

Complex oxides exhibiting pronounced proton-conducting behaviour are attracting great attention as functional materials, i.e. electrolyte ceramic membranes for various types of solid oxide electrochemical devices, such as fuel cells, electrolysis cells, sensors/pumps, converters etc. [1–7].

In the most common cases [8,9], proton transport results from the interaction of steam with oxygen vacancies of an oxide (Eq. (1)), when an impurity disordering is realised by means of an acceptor-doping strategy (Eq. (2)).

$$H_2O + V_O^{\bullet\bullet} + O_O^x \rightleftarrows 2OH_O^{\bullet}, \quad (1)$$

$$R_2O_3 \xrightarrow{"BO_2" \text{ of } ABO_3} 2R_B^{/} + V_O^{\bullet\bullet} + 3O_O^x, \quad (2)$$

where: $V_O^{\bullet\bullet}$ is the oxygen vacancies, O_O^x is the oxygen-ion in its a regular position, $R_B^{/}$ is the impurity (acceptor) defect, $OH_O^{\bullet}$ is the proton localised at the oxygen-ion.

Concentration of the formed protons depends on many factors, including the inherent properties of the oxides and external parameters [10–12], leading to the highest levels of proton conductivity for barium cerate ($BaCeO_3$) and barium zirconate ($BaZrO_3$) materials. As a result, Ba(Ce,Zr)O_3-based electrolytes have found the widest application in the mentioned electrochemical devices [13–15]. Despite significantly promising results obtained in their application in such devices [16–18], the Ba-based compounds are compromised by the formation of $BaCO_3$ impurities, which have been confirmed even for a high-tolerance $BaZrO_3$ phase [19–21]. Therefore, when designing functional materials with a low concentration (or absence) of alkaline-earth elements, one of the current strategies is to achieve a high chemical stability of oxides in terms of their carbonisation [22].

A series of Ln-based oxide phases, which are also capable of demonstrating significant proton transport, are the subject of current research. Some of these phases belong to the class of mixed ionic(protonic)-electronic conductors or MIECs [23–26]: $Ln_{6-x}MoO_{12-\delta}$, $Ln_2ScTaO_{7-\delta}$, $Ln_6WO_{12-\delta}$. An additional series of primarily lanthanum-based materials can show predominant proton conductivity under certain conditions [27–31]: $La_2Zr_2O_7$, $LaNbO_4$, $LaNb_3O_9$, $LaREO_3$ (RE = Sc, Y, Yb). Among these, $LaYO_3$ and $LaYbO_3$ are positioned as promising proton-conducting electrolytes [32–35], having been successfully utilised in such electrochemical systems as hydrogen sensors and hydrogen pumps [36,37].

In the present work, we present results of the experimental preparation and characterisation of $La_{1-x}Ba_xYbO_{3-\delta}$ ceramic materials having a reduced Ba-content. Although the Ba-doped $LaYbO_3$ system has been the subject of a recent study, particularly in terms of hydration

* Corresponding authors at: Institute of High Temperature Electrochemistry, 620137, Yekaterinburg, Russia.
E-mail addresses: yulia.lyagaeva@ya.ru (J.G. Lyagaeva), dmitrymedv@mail.ru (D.A. Medvedev).

https://doi.org/10.1016/j.jeurceramsoc.2019.09.005
Received 15 May 2019; Received in revised form 26 August 2019; Accepted 3 September 2019
Available online 07 September 2019

capability and proton concentration [35], these data are associated with the bulk properties of the system. By contrast, the present work also reveals the effects of morphological and microstructural parameters on grain boundary and overall transport.

2. Experimental details

2.1. Synthesis of materials

The $La_{1-x}Ba_xYbO_{3-\delta}$ (where x = 0.03, 0.05 and 0.1) materials were synthesised via citrate-nitrate combustion synthesis. In detail, $La(NO_3)_3{\cdot}6H_2O$, $Ba(NO_3)_2$, $Yb(NO_3)_3{\cdot}5H_2O$ in powder form were measured in strictly stoichiometric amounts and dissolved in distilled water until the formation of a transparent solution. Citric acid was added to this solution heated to 80 °C, adjusting the total amount of cations to a mole ratio of 2:1, respectively. Next, ammonia solution was added to bring the pH parameter of the resulting solution close to 7 (pH neutral). The final solution was heated at 250 °C using a hotplate to initiate the following process sequence: active water evaporation, the formation of sol-gel, its self-ignition and the subsequent formation of sponge-like highly dispersed powders (see supplementary materials, Fig. S1).

In order to determine the optimal synthesis regime (1100 °C for 5 h), the as-obtained powders were analysed by thermogravimetric (TG) analysis coupled with differential scanning calorimetry (DSC). Following synthesis at the selected temperature for 5 h, the powders were uniaxially pressed at 250 MPa and studied by means of high-temperature dilatometry technique to reveal the Ba-doping effect on the densification behaviour. On the basis of these data, the sintering regime (1400 °C for 5 h) was additionally optimised for obtaining the ceramic samples.

2.2. Characterisation of materials

TG-DSC study was performed on the STA 449 F3 Jupiter, Netzsch thermal analyser in static air with temperature variation from room temperature (RT) up to 1200 °C with a heating rate of 10 °C min^{-1}. A dilatometry study was carried out using a Netzsch DIL 402 PC dilatometer. The scans of the pressed synthesised powders were performed in a range of RT–1400 °C with a cooling rate of 5 °C min^{-1}.

The phase composition of the sintered ceramic samples and the refinement of unit cell parameters were carried out by X-ray diffraction analysis (XRD, Rigaku D/MAX-2200VL/PC) and Rietveld analysis (using Fullprof software), respectively.

The morphology of the ceramic samples was observed by means of a TESCAN MIRA 3 LMU scanning electron microscope and then statistically analysed by a ImageJ software.

2.3. Materials functional properties

The phase stability of $La_{1-x}Ba_xYbO_{3-\delta}$ was studied for the powder samples treated under pure 100% CO_2 at 700 °C for 5 h and then analysed by XRD.

The thermal expansion behaviour of $La_{1-x}Ba_xYbO_{3-\delta}$ was studied in the range of 100–1000 °C in a wet air atmosphere under cooling mode using the dilatometry data.

The total conductivity of the sample, as well as the bulk and grain boundary contributions, was measured by means of electrochemical impedance spectroscopy (EIS) using a complex of techniques including an Amel 2550 potentiostat/galvanostat and Materials M520 FRA-box. These measurements were performed within a 200–600 °C temperature range in wet air atmosphere, under which conditions the samples exhibit predominant proton conducting behaviour. The obtained spectra were analysed using an equivalent circuits method and refined by means of the distribution of relaxation times (DRT) method using the DRTtools software [38–40].

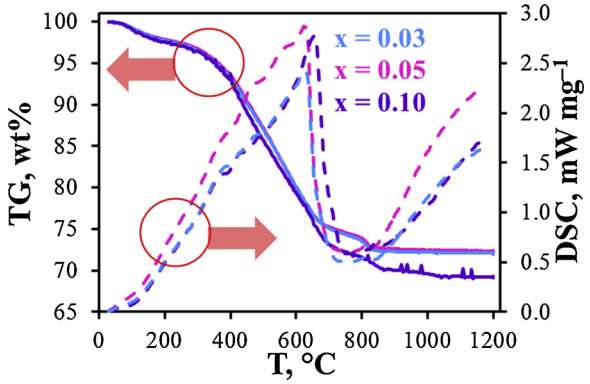

Fig. 1. TG-DSC results of the as-combusted $La_{1-x}Ba_xYbO_{3-\delta}$ powders.

Table 1
Ceramic properties of the $La_{1-x}Ba_xYbO_{3-\delta}$ materials sintered at 1400 °C for 5 h: L is the total shrinkage, ρ is the relative density, D is the mean grain size, p is the open porosity.

x	L, %	ρ, %	D ± 5%, μm	p[c], %
0.03	17.5[a]	96.7	0.33	–
0.05	14.2[b]	92.2	0.65	–
0.1	4.7[a]	75.9	0.88	9.5

[a] Measured by dilatometry technique (Fig. S2).
[b] Measured by a direct comparison of linear parameters of the sample before and after its sintering.
[c] The open porosity was evaluated as an area ratio between white and black regions (Fig. 2c).

3. Results and discussion

3.1. Preparation of ceramics

The powders comprising the source of ceramic materials were produced by the citrate-nitrate combustion synthesis route. This has many advantages over solid-state synthesis methods, including improved homogeneity and the nano-sized character of the powders [41–43], allowing the achievement of single-phase and dense materials at reduced synthesis and sintering temperatures. During this process, the following redox reaction occurs (presented without water crystallisation):

$$(1-x)La(NO_3)_3 + xBa(NO_3)_2 + Yb(NO_3)_3 + \varphi\gamma C_6H_8O_7 \rightarrow$$
$$\rightarrow La_{1-x}Ba_xYbO_{3-x/2} + 6\varphi\gamma CO_2\uparrow + (3-0.5x)N_2\uparrow + 4\varphi\gamma H_2O\uparrow \quad (3)$$

Here, φ is the stoichiometric amount of a fuel (citric acid), which is equal to about 3, assuming that no free oxygen participates in the combustion process; γ is the correction factor, used for setting the mentioned ratio between total amount of cations and the fuel (γ = 4/3). As can be seen, this process is accompanied by the release of a large quantity of gases, which promotes the formation of highly disperse powders, Fig. S1. These as-combusted powders contain the residue of organic substances, whose concentration exceeds 20 wt% (Fig. 1). As evaluated by calcination in ambient air, the main weight loss of such powders occurs at 300–800 °C, when the full oxidation of the organic substances with a pronounced exothermic effect can be observed. The weight of the powders stabilises at temperatures above 1050 °C, at which point the last carbon-containing compound is removed (CO_2 as a product of the $BaCO_3$ decomposition).

Based on the TG-DSC analysis, a temperature of 1100 °C with a dwell time of 5 h was selected for production of carbon-free powders. These were then pressed and characterised by dilatometry technique and relative density measurements in order to study the sintering behaviour (Fig. S2, Table 1). The dilatometry data were obtained at

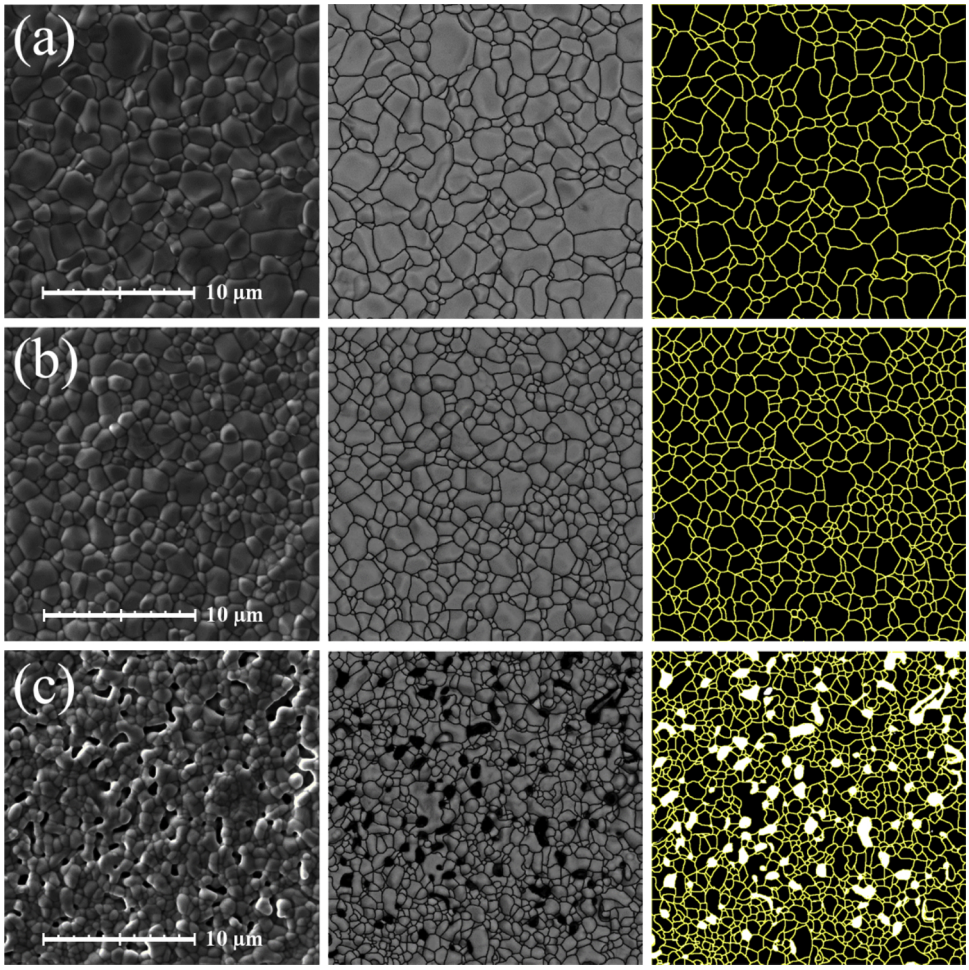

Fig. 2. Surface morphology in secondary electron imaging mode (left), grain boundary detection (centre) and image binarisation (right) for the $La_{1-x}Ba_xYbO_{3-\delta}$ sintered ceramic materials: x = 0.03 (a), x = 0.05 (b) and x = 0.10 (c). The pores are shown as white objects.

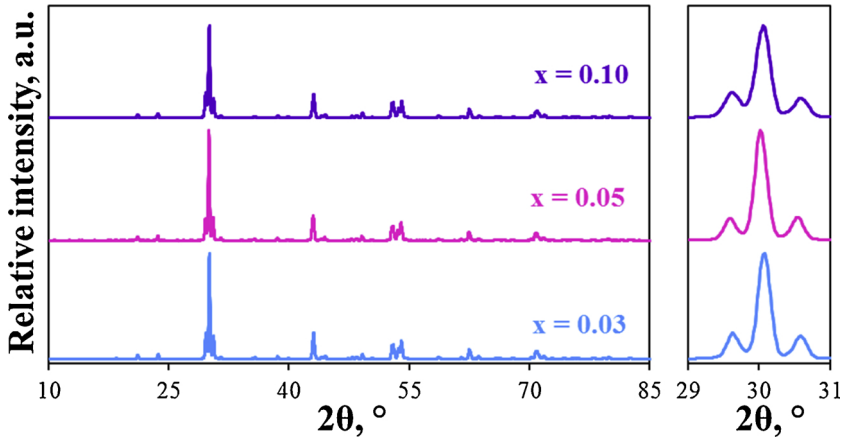

Fig. 3. XRD patterns of the sintered $La_{1-x}Ba_xYbO_{3-\delta}$ materials.

Table 2
Refined unit cell parameters of the sintered $La_{1-x}Ba_xYbO_{3-\delta}$ materials.

x	A ±0.001, Å	b ±0.001, Å	c ±0.001, Å	V ±0.14, Å^3
0.03	6.025	5.842	8.410	296.02
0.05	6.024	5.842	8.415	296.14
0.10	6.025	5.839	8.417	296.11

temperatures below 1450 °C, when only an orthorhombic modification of $LaYbO_3$ is stable. The Ba-doping leads to a deterioration of the densification of the ceramics, which is confirmed by the total shrinkage parameter, Table 1. The relative density of the samples sintered at the selected temperature (1400 °C) for 5 h also decreases, from ~97% for x = 0.03 to ~76% for x = 0.1.

To evaluate such microstructural parameters as mean grain size (D) and open porosity (p), the sintered samples were characterised by SEM analysis followed by processing of the obtained images using ImageJ

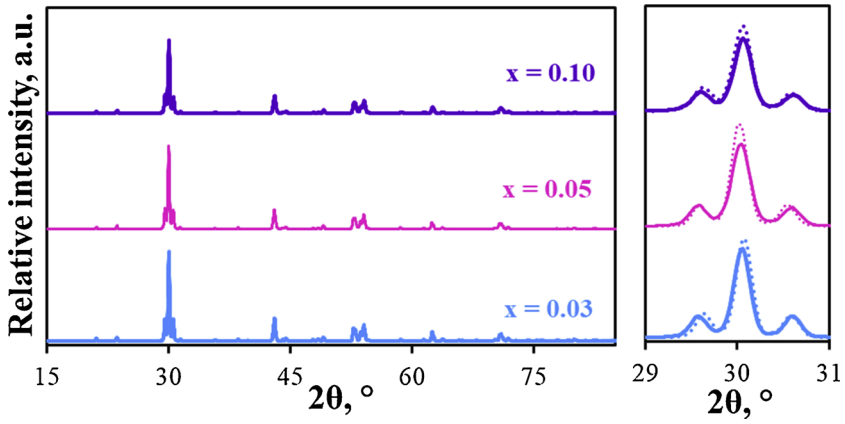

Fig. 4. XRD patterns of the $La_{1-x}Ba_xYbO_{3-\delta}$ powders treated in the CO_2 flow at 700 °C for 5 h. The dotted lines in the detailed region correspond to the XRD patterns of the sintered materials.

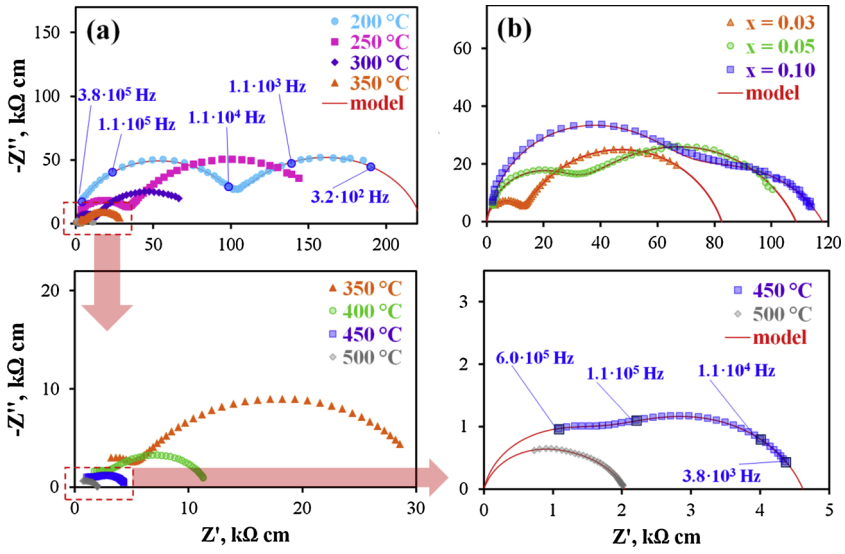

Fig. 5. Typical impedance spectra obtained for the symmetrical cell in wet air atmospheres: for $La_{0.97}Ba_{0.03}YbO_{3-\delta}$ at various temperatures (a) and for $La_{1-x}Ba_xYbO_{3-\delta}$ at 300 °C (b).

software (Fig. 2). The D value decreases with increased Ba-concentration, while the p value is close to null for x = 0.03 and 0.05 and amounts to ~10% for x = 0.1. Both of these tendencies confirm the deteriorated densification of the samples caused by Ba-doping.

It is worth mentioning that a highly dense structure with close-packed grains was formed for the samples with x = 0.03 and 0.05, when a low sintering temperature of 1400 °C was used. According to an analysis of the literature data, the densification of $LaYbO_3$-based ceramic materials at reduced temperatures is a similarly challenging task. For example, Obukuro et al. [35] fabricated dense $La_{1-x}Ba_xYbO_{3-\delta}$ samples using a high temperature (1700 °C) and dwell time (10 h). Feteira et al. [44] obtained a non-porous $LaYbO_3$ sample (97% of relative density) at 1600 °C for 4 h in case of no Ba-modification. Therefore, the combustion synthesis method utilised in this work allows good ceramic properties to be achieved, with a clear economic benefit coming from the lower energy requirement.

The structural parameters of $La_{1-x}Ba_xYbO_{3-\delta}$ (following section) were analysed for the obtained powders by milling the corresponding ceramic materials in order to confirm their single-phase nature.

3.2. Crystal structure

Fig. 3 shows the XRD results, which demonstrate the formation of a perovskite structure having an orthorhombic distortion for all the studied samples. Principally, $LaYbO_3$ can be indexed within either the $Pna2_1$ [45,46] or Pnma space group [44,47,48]. In order to clarify the nature of the formed structure, a Rietveld analysis was performed (Figs. S3 and S4). These data show that an improved agreement is reached for the first symmetry, while the difference between experimental and calculated profiles, presented in the form of reliability factors (R_p, R_{wp}, χ^2), is considerably higher for the latter symmetry (Fig. S3). It is interesting to note that problems concerning the correct description of the $LaYbO_3$ structure have been recently considered [44]. The authors of this study, which used three possible space groups (Pnma, Cmcm and $Pna2_1$), revealed that the best refinement was observed for the Pnma space group. It is likely that the realisation of a certain symmetry depends on different factors, including sintering temperatures, presence of uncontrollable purities in the powder sources and even the level of water partial pressure (pH_2O) in air under the technological regimes. In detail, the pH_2O parameter determines the hydration capability of the materials, which can result in a chemical strain and changes in the symmetry of the crystal structure [8,49].

Returning to the present results, all the representatives of $La_{1-x}Ba_xYbO_{3-\delta}$ were indexed in the $Pna2_1$ space group (Fig. S4) with the refined unit cell parameters as presented in Table 2. The majority of the parameters are virtually unchanged, with increased Ba-concentration leading to almost the same unit cell volume, 296.08 ± 0.20 $Å^3$. This tendency can be attributed to a low degree of La^{3+} with Ba^{2+}

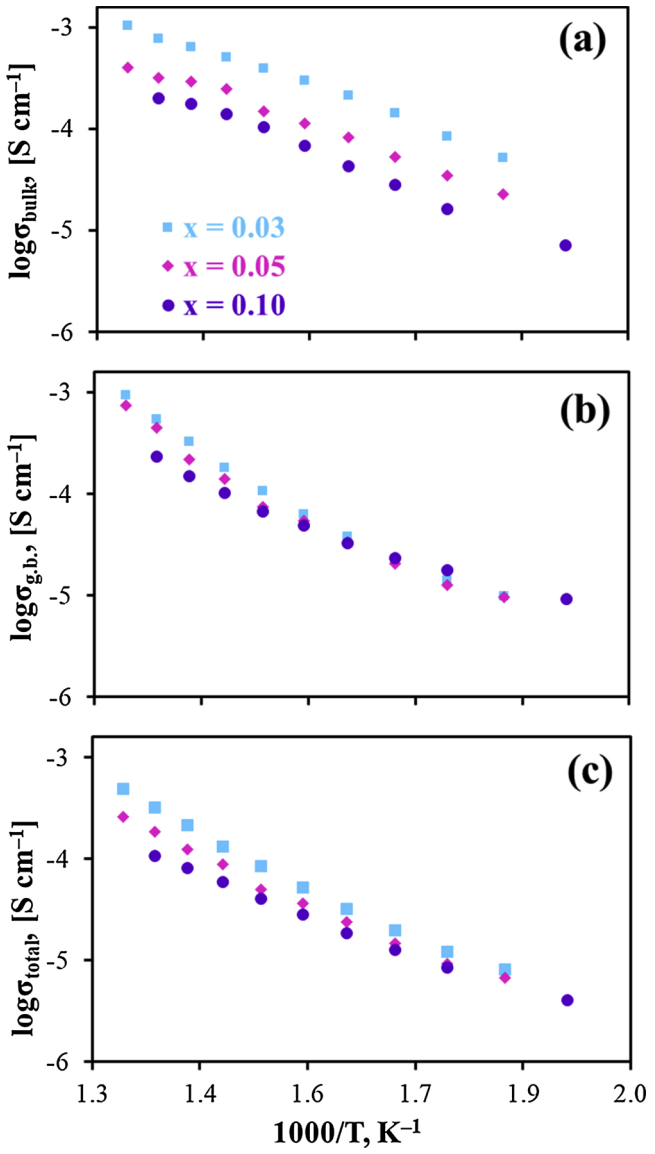

Fig. 6. Bulk (a), grain boundary (b) and total (c) conductivities of the $La_{1-x}Ba_xYbO_{3-\delta}$ ceramic materials in wet air atmosphere depending on reciprocal temperature.

substitution despite the differing ionic radii of host and guest ions – 1.36 and 1.61 Å, respectively [50].

3.3. Chemical stability

As mentioned above, the La-based proton conductors show a higher chemical stability than conventional $BaCeO_3$-based analogues. In order to verify this assumption, the $La_{1-x}Ba_xYbO_{3-\delta}$ powders were kept in a pure atmosphere of CO_2 for 5 h prior to a characterisation of their phase structure (Fig. 4). No secondary phases in detectable amounts were found following such a treatment; moreover, no meaningful displacement of the XRD reflexes was detected. Both of these results indicate that the studied materials exhibit the desirable stability in CO_2-containing atmospheres. This permits the use of such materials as electrolytes for the various electrochemical and conversion processes in which CO_2 participates as a reagent or product [51–54].

3.4. Electrical properties

The transport properties of the sintered materials at low temperatures were evaluated by means of the EIS analysis (Fig. 5) at temperature and frequency ranges within which the bulk and grain boundary processes can be clearly separated. Such a separation was performed using an equivalent scheme of $R_o – R_1Q_1 – R_2Q_2$, where R_o is the correction parameter (0.001 Ω cm), imitating the origin of the coordinates; R_1 and R_2 are the bulk and grain boundary resistances; and Q_1 and Q_2 are the corresponding constant phase elements. The model curves agree well with the experimental data, as can be seen from the examples presented in Fig. 5.

The partial resistances were correlated with the corresponding processes in order to calculate the capacitance values ($C = (R{\cdot}Q)^{1/n}/R$), which were equal about $(1–5){\cdot}10^{-11}$ and $(2–7){\cdot}10^{-9}$ F cm^{-1} for the first and second semicircles. Next, the total resistance was derived as a sum of R_1 and R_2. The total and partial conductivities were finally calculated using the dimension parameters of the symmetrical cells:

$$\sigma_j = \frac{1}{R_j}\cdot\frac{h}{S} \quad (4)$$

where h is the thickness of the electrolyte disc, S is the electrode area, j = 1, 2 or total.

Fig. 6 displays the transport properties of the $La_{1-x}Ba_xYbO_{3-\delta}$ materials. The grain boundaries determine the overall transport of ytterbates for almost all studied conditions (Fig. S5). At the same time, the grain boundary conductivity varies slightly with the Ba-doping (less than a half order of magnitude, Fig. 6b), despite considerable changes in microstructural parameters (grain size, porosity, Table 1). This fact might be associated with the following reasons: the grain boundary

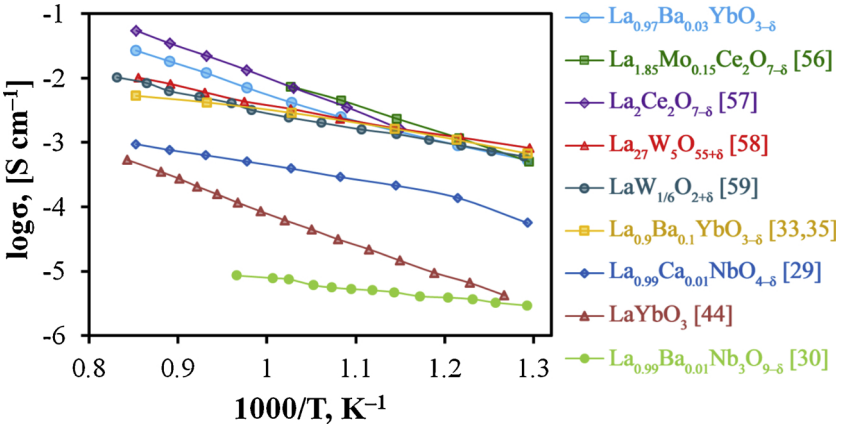

Fig. 7. Total conductivity of the $La_{0.97}Ba_{0.03}YbO_{3-\delta}$ ceramic material in wet air atmosphere compared with a number of La-based oxides demonstrating proton transportation.

region is quite pure and the dopant (or phase) segregation is insignificant with increased Ba-concentration.

As shown in Fig. 6a, the bulk conductivity is a more sensitive parameter associated with variation in composition, resulting in a difference of ~1 order of magnitude. This tendency agrees with the recent data of Obukuro et al. [35]; in this study, the authors revealed a similar (inverse) correlation between proton mobility and x in $La_{1-x}Ba_xYbO_{3-\delta}$, which arises from the defect association effect (when protons are trapped by the acceptor dopants [12,55]). Realising proton transportation in grains is confirmed by the calculated activation energy (E_a), which is rather low (equal to 0.56 ± 0.06 eV for all three samples).

The resulting total conductivity decreases with an increase in the Ba-concentration, for example, from 0.32 mS cm^{-1} for x = 0.03 to 0.11 mS cm^{-1} for x = 0.10 (at 475 °C), while the E_a drops from 0.75 eV to 0.60 eV (at the whole low-temperature range), respectively. Therefore, the bulk properties affect the overall transport of the ceramic materials in a higher degree than the grain boundary properties, although the contribution of the latter predominates.

The transport properties of $La_{1-x}Ba_xYbO_{3-\delta}$ were also studied via a 4-probe DC technique between 500 and 900 °C, when no separation of bulk and grain boundary resistances can be performed. As discussed earlier, these data are in good agreement with EIS (Fig. S6). The total conductivity is found to decrease with increasing x in the studied system (Fig. 7), being in qualitative agreement with the bulk properties. This is because the grain boundaries cease to be a determining factor at temperatures higher than 500 °C (Fig. S5). However, the E_a values increase up to 0.86–0.91 eV, indicating the change of electrical behaviour, most probably from proton to oxygen-ion transportation. To confirm this assumption, the total conductivity of the nominally pure $LaYbO_3$ is also presented [44]. Since it does not contain acceptor dopants, the oxygen-ionic conductivity of lanthanum ytterbate is very low, has E_a about 0.97 eV and is determined by a disordering of its structure. At the same time, the obtained data were also compared with those obtained for the highly doped oxide (x = 0.10 [33,35]). According to the literature results, its E_a reaches ~0.65 eV, although only 15% of oxygen vacancies at 800–900 °C were hydrated. Such an apparently very low activation energy requires future verification.

To sum up, the conductivity of the sample with x = 0.03 attains 0.53, 1.51, 4.18, 12.0 and 27.1 S cm^{-1} at 500, 600, 700, 800 and 900 °C, respectively. These levels are comparable with the conductivity not only of state-of-the-art La-based proton-conducting oxides [56–59], but also of the Zr-enriched $BaCeO_3$–$BaZrO_3$-based electrolytes [13,15,60], which allows $La_{0.97}Ba_{0.03}YbO_{3-\delta}$ to be considered as a CO_2-tolerant proton-conducting electrolyte.

4. Conclusions

In the present work, a suitable combustion synthesis method was developed in order to obtain single-phase $La_{1-x}Ba_xYbO_{3-\delta}$ proton-conducting materials. The highly dense ceramic samples can be prepared at a reduced sintering temperature (1400 °C) in the case of a low Ba-concentration (not more than x = 0.05). The XRD analysis shows the relatively high tolerance of ytterbates towards carbonisation, since their phase structure does not change before and after treatment in pure CO_2 at 700 °C for 5 h. According to electrical measurements, the transport properties of $La_{1-x}Ba_xYbO_{3-\delta}$ are determined by grain boundaries across a low temperature range (200–500 °C), while bulk transport predominates at higher temperatures. Changing x in the studied system affects bulk transport to a greater extent than grain boundary transport, which results in a general regularity consisting in the deterioration of transport properties with Ba-doping. Nevertheless, even $La_{0.97}Ba_{0.03}YbO_{3-\delta}$ with a low impurity disordering structure has acceptable conductivity levels varying from ~1.5 mS cm^{-1} at 600 °C to ~12 mS cm^{-1} at 800 °C.

Acknowledgment

The presented results were performed within the framework of the budgetary plans of the Institute of High Temperature Electrochemistry (IHTE).

The characterisation of powder and ceramic materials was carried out at the Shared Access Centre “Composition of Compounds” of IHTE [61].

Appendix A. Supplementary data

Supplementary material related to this article can be found, in the online version, at doi:https://doi.org/10.1016/j.jeurceramsoc.2019.09.005.

References

[1] S. Hossain, A.M. Abdalla, S.N.B. Jamain, J.H. Zaini, A.K. Azad, A review on proton conducting electrolytes for clean energy and intermediate temperature-solid oxide fuel cells, Renew. Sustain. Energy Rev. 79 (2017) 750–764, https://doi.org/10.1016/j.rser.2017.05.147.
[2] S.P. Cardoso, I.S. Azenha, Z. Lin, I. Portugal, A.E. Rodrigues, C.M. Silva, Inorganic membranes for hydrogen separation, Separat. Purif. Rev. 47 (2018) 229–266, https://doi.org/10.1080/15422119.2017.1383917.
[3] A. Volkov, E. Gorbova, A. Vylkov, D. Medvedev, A. Demin, P. Tsiakaras, Design and applications of potentiometric sensors based on proton-conducting ceramic materials. A brief review, Sens. Actuators B Chem. 244 (2017) 1004–1015, https://doi.org/10.1016/j.snb.2017.01.097.
[4] A. Afif, N. Radenahmad, Q. Cheok, S. Shams, J.H. Kim, A.K. Azad, Ammonia-fed fuel cells: a comprehensive review, Renew. Sust. Energy Rev. 60 (2016) 822–835, https://doi.org/10.1016/j.rser.2016.01.120.
[5] Z. Tao, L. Yan, J. Qiao, B. Wang, L. Zhang, J. Zhang, A review of advanced proton-conducting materials for hydrogen separation, Prog. Mater. Sci. 74 (2015) 1–50, https://doi.org/10.1016/j.pmatsci.2015.04.002.
[6] L. Bi, S. Boulfrad, E. Traversa, Steam electrolysis by solid oxide electrolysis cells (SOECs) with proton-conducting oxides, Chem. Soc. Rev. 43 (2014) 8255–8270, https://doi.org/10.1039/C4CS00194J.
[7] S.S. Hashim, M.R. Somalu, K.S. Loh, S. Liu, W. Zhou, J. Sunarso, Perovskite-based proton conducting membranes for hydrogen separation: a review, Int. J. Hydrogen Energy 43 (2018) 15281–15305, https://doi.org/10.1016/j.ijhydene.2018.06.045.
[8] W. Wang, D. Medvedev, Z. Shao, Gas humidification impact on the properties and performance of perovskite-type functional materials in proton-conducting solid oxide cells, Adv. Funct. Mater. 28 (2018) 1802592, , https://doi.org/10.1002/adfm.201802592.
[9] P. Colomban, Proton and Protonic Species: The Hidden Face of Solid State Chemistry. How to Measure H Content in Materials? Fuel Cells 13 (2013) 6–18, https://doi.org/10.1002/fuce.201200088.
[10] K.D. Kreuer, Proton-conducting oxides, Annu. Rev. Mater. Res. 33 (2003) 333–359, https://doi.org/10.1146/annurev.matsci.33.022802.091825.
[11] L. Malavasi, C.A.J. Fisher, M.S. Islam, Oxide-ion and proton conducting electrolyte materials for clean energy applications: structural and mechanistic features, Chem. Soc. Rev. 39 (2010) 4370–4387, https://doi.org/10.1039/B915141A.
[12] L.P. Putilov, V.I. Tsidilkovski, Impact of bound ionic defects on the hydration of acceptor-doped proton-conducting perovskites, Phys. Chem. Chem. Phys. 21 (2019) 6391–6406, https://doi.org/10.1039/C8CP07745B.
[13] D.A. Medvedev, J.G. Lyagaeva, E.V. Gorbova, A.K. Demin, P. Tsiakaras, Advanced materials for SOFC application: Strategies for the development of highly conductive and stable solid oxide proton electrolytes, Prog. Mater. Sci. 75 (2016) 38–79, https://doi.org/10.1016/j.pmatsci.2015.08.001.
[14] H. Dai, H. Kou, H. Wang, L. Bi, Electrochemical performance of protonic ceramic fuel cells with stable $BaZrO_3$-based electrolyte: a mini-review, Electrochem. Commun. 96 (2018) 11–15, https://doi.org/10.1016/j.elecom.2018.09.001.
[15] D.A. Medvedev, J.G. Lyagaeva, E.V. Gorbova, A.K. Demin, P. Tsiakaras, Advanced materials for SOFC application: Strategies for the development of highly conductive and stable solid oxide proton electrolytes, Prog. Mater. Sci. 75 (2016) 38–79, https://doi.org/10.1016/j.pmatsci.2015.08.001.
[16] H. An, H. Lee, B. Kim, J. Son, K.J. Yoon, H. Kim, D. Shin, H. Ji, J. Lee, A 5 × 5 cm^2 protonic ceramic fuel cell with a power density of 1.3 W cm^{-2} at 600 °C, Nat. Energy 3 (2018) 870–875, https://doi.org/10.1038/s41560-018-0230-0.
[17] C. Duan, R. Kee, H. Zhu, N. Sullivan, L. Zhu, L. Bian, D. Jennings, R. O'Hayre, Highly efficient reversible protonic ceramic electrochemical cells for power generation and fuel production, Nat. Energy 4 (2019) 230–240, https://doi.org/10.1038/s41560-019-0333-2.
[18] H. Malerød-Fjeld, D. Clark, I. Yuste-Tirados, R. Zanón, D. Catalán-Martinez, D. Beeaff, S.H. Morejudo, Per K. Vestre, T. Norby, R. Haugsrud, J.M. Serra, C. Kjølseth, Thermo-electrochemical production of compressed hydrogen from methane with near-zero energy loss, Nat. Energy 2 (2017) 923–931, https://doi.org/10.1038/s41560-017-0029-4.
[19] R. Sažinas, C. Bernuy-López, M.-A. Einarsrud, T. Grande, Effect of CO_2 exposure on the chemical stability and mechanical properties of $BaZrO_3$ ceramics, J. Am. Ceram.

Soc. 99 (2006) 3685–3695, https://doi.org/10.1111/jace.14395.
[20] J.M. Polfus, J. Yang, B. Yildiz, Interplay between H_2O and CO_2 coadsorption and space-charge on Y-doped $BaZrO_3$ surfaces, J. Mater. Chem. A 6 (2018) 24823–24830, https://doi.org/10.1039/C8TA09491H.
[21] R. Sažinas, M.F. Sunding, A. Thøgersen, I. Sakaguchi, T. Norby, T. Grandea, J.M. Polfus, Surface reactivity and cation non-stoichiometry in $BaZr_{1-x}Y_xO_{3-\delta}$ (x = 0–0.2) exposed to CO_2 at elevated temperature, J. Mater. Chem. A 7 (2019) 3848–3856, https://doi.org/10.1039/C8TA11021B.
[22] Y. Chen, W. Zhou, D. Ding, M. Liu, F. Ciucci, M. Tade, Z. Shao, Advances in cathode materials for solid oxide fuel cells: complex oxides without alkaline earth metal elements, Adv. Energy Mater. 5 (2015) 1500537, , https://doi.org/10.1002/aenm.201500537.
[23] A.V. Shlyakhtina, I.V. Kolbanev, E.N. Degtyarev, N.V. Lyskov, O.K. Karyagina, S.A. Chernyak, L.G. Shcherbakova, Kinetic aspects of the synthesis of $Ln_{6-x}MoO_{12-\delta}$ (Ln = Sm, Ho -Yb; x = 0, 0.5) rare-earth molybdates using mechanical activation of oxides, Solid State Ion. 320 (2018) 272–282, https://doi.org/10.1016/j.ssi.2018.02.004.
[24] A.V. Shlyakhtina, S.N. Savvin, N.V. Lyskov, D.A. Belov, A.N. Shchegolikhin, I.V. Kolbanev, O.K. Karyagina, S.A. Chernyak, L.G. Shcherbakova, P. Núñez, $Sm_{6-x}MoO_{12-\delta}$ (x = 0, 0.5) and Sm_6WO_{12} – mixed electron-proton conducting materials, Solid State Ion. 302 (2017) 143–151, https://doi.org/10.1016/j.ssi.2017.01.020.
[25] S. Escolástico, C. Solís, T. Scherb, G. Schumacher, J.M. Serra, Hydrogen separation in $La_{5.5}WO_{11.25-\delta}$ membranes, J. Membr. Sci. 444 (2013) 276–284, https://doi.org/10.1016/j.memsci.2013.05.005.
[26] A.V. Shlyakhtina, M. Avdeev, J.C.C. Abrantes, E. Gomes, N.V. Lyskov, E.P. Kharitonova, I.V. Kolbaneva, L.G. Shcherbakova, Structure and conductivity of $Nd6MoO_{12}$-based potential electron–proton conductors under dry and wet redox conditions, Inorg. Chem. Front. 6 (2019) 566–575, https://doi.org/10.1039/C8QI01142G.
[27] T. Omata, K. Ikeda, R. Tokashiki, S. Otsuka-Yao-Matsuo, Proton solubility for $La_2Zr_2O_7$ with a pyrochlore structure doped with a series of alkaline-earth ions, Solid State Ion. 167 (2004) 389–397, https://doi.org/10.1016/j.ssi.2004.01.015.
[28] S. Wachowski, B. Kamecki, P. Winiarz, K. Dzierzgowski, A. Mielewczyk-Gryńa, M. Gazda, Tailoring structural properties of lanthanum orthoniobates through an isovalent substitution on the Nb-site, Inorg. Chem. Front. 5 (2018) 2157–2166, https://doi.org/10.1039/C8QI00524A.
[29] L. Hakimova, A. Kasyanova, A. Farlenkov, J. Lyagaeva, D. Medvedev, A. Demin, P. Tsiakaras, Effect of isovalent substitution of La^{3+} in Ca-doped $LaNbO_4$ on the thermal and electrical properties, Ceram. Int. 45 (2019) 209–215, https://doi.org/10.1016/j.ceramint.2018.09.153.
[30] I. Animitsa, A. Iakovleva, K. Belova, Electrical properties and water incorporation in A-site deficient perovskite $La_{1-x}Ba_xNb_3O_{9-0.5X}$, J. Solid State Chem. 238 (2016) 156–161, https://doi.org/10.1016/j.jssc.2016.03.023.
[31] A.V. Kuzmin, A.Y. Stroeva, V.P. Gorelov, Y. Novikova, A.S. Lesnichyova, A.S. Farlenkov, A.V. Khodimchuk, Synthesis and characterization of dense proton-conducting $La_{1-x}Sr_xScO_{3-\alpha}$ ceramics, Int. J. Hydrogen Energy 44 (2019) 1130–1138, https://doi.org/10.1016/j.ijhydene.2018.11.041.
[32] Y. Okuyama, T. Kozai, S. Ikeda, M. Matsuka, T. Sakai, H. Matsumoto, Incorporation and conduction of proton in Sr-doped $LaMO_3$ (M = Al, Sc, In, Yb, Y), Electrochim. Acta 125 (2014) 443–449, https://doi.org/10.1016/j.electacta.2014.01.113.
[33] Y. Okuyama, T. Kozai, T. Sakai, M. Matsuka, H. Matsumoto, Proton transport properties of $La_{0.9}M_{0.1}YbO_{3-\delta}$ (M = Ba, Sr, Ca, Mg), Electrochim. Acta 95 (2013) 54–59, https://doi.org/10.1016/j.electacta.2013.01.156.
[34] N. Danilov, G. Vdovin, O. Reznitskikh, D. Medvedev, A. Demin, P. Tsiakaras, Physico-chemical characterization and transport features of proton-conducting Sr-doped $LaYO_3$ electrolyte ceramics, J. Eur. Ceram. Soc. 36 (2016) 2795–2800, https://doi.org/10.1016/j.jeurceramsoc.2016.04.018.
[35] Y. Obukuro, Y. Okuyama, G. Sakai, S. Matsushima, Experimental and theoretical approaches for the investigation of proton conductive characteristics of $La_{1-x}Ba_xYbO_{3-\delta}$, J. Alloys. Compd. 770 (2019) 294–300, https://doi.org/10.1016/j.jallcom.2018.08.062.
[36] A. Kalyakin, J. Lyagaeva, D. Medvedev, A. Volkov, A. Demin, P. Tsiakaras, Characterization of proton-conducting electrolyte based on $La_{0.9}Sr_{0.1}YO_{3-\delta}$ and its application in a hydrogen amperometric sensor, Sens. Actuators B Chem. 225 (2016) 446–452, https://doi.org/10.1016/j.snb.2015.11.064.
[37] T. Sakai, K. Isa, M. Matsuka, T. Kozai, Y. Okuyama, T. Ishihara, H. Matsumoto, Electrochemical hydrogen pumps using Ba doped $LaYbO_3$ type proton conducting electrolyte, Int. J. Hydrogen Energy 38 (2013) 6842–6847, https://doi.org/10.1016/j.ijhydene.2013.03.050.
[38] B.A. Boukamp, Fourier transform distribution function of relaxation times; application and limitations, Electrochimi. Acta 154 (2015) 35–46, https://doi.org/10.1016/j.electacta.2014.12.059.
[39] F. Ciucci, C. Chen, Analysis of electrochemical impedance spectroscopy data using the distribution of relaxation times: a bayesian and hierarchical bayesian approach, Electrochim. Acta 167 (2015) 439–454, https://doi.org/10.1016/j.electacta.2015.03.123.
[40] T.H. Wan, M. Saccoccio, C. Chen, F. Ciucci, Influence of the discretization methods on the distribution of relaxation times deconvolution: implementing radial basis functions with DRTtools, Electrochim. Acta 184 (2015) 483–499, https://doi.org/10.1016/j.electacta.2015.09.097.
[41] Z. Shao, W. Zhou, Z. Zhu, Advanced synthesis of materials for intermediate-temperature solid oxide fuel cells, Prog. Mater. Sci. 57 (2012) 804–874, https://doi.org/10.1016/j.pmatsci.2011.08.002.
[42] L. Fan, B. Zhu, P.-C. Su, C. He, Nanomaterials and technologies for low temperature solid oxide fuel cells: recent advances, challenges and opportunities, Nano Energy 45 (2018) 148–176, https://doi.org/10.1016/j.nanoen.2017.12.044.
[43] A. Varma, A.S. Mukasyan, A.S. Rogachev, K.V. Manukyan, Solution combustion synthesis of nanoscale materials, Chem. Rev. 116 (2016) 14493–14586, https://doi.org/10.1021/acs.chemrev.6b00279.
[44] A. Feteira, L.J. Gillie, R. Elsebrock, D.C. Sinclair, Crystal structure and dielectric properties of $LaYbO_3$, J. Am. Ceram. Soc. 90 (2007) 1475–1482, https://doi.org/10.1111/j.1551-2916.2007.01549.x.
[45] H. Müller-Buschbaum, C. Teske, Zur Kenntnis Der Kristallstruktur von $LaYbO_3$, J. Inorg. General. Chem. 369 (1969) 225–264, https://doi.org/10.1002/zaac.19693690316.
[46] E. Ruiz-Trejo, M.S. Islam, J.A. Kilner, Atomistic simulation of defects and ion migration in $LaYO_3$, Solid State Ion. 123 (1999) 121–129, https://doi.org/10.1016/S0167-2738(99)00092-2.
[47] A. Cabrera, F.E. Charry, J.R. Rojas, D.A. Landinez, F. Fajardo, Synthesis, structural and morphological characterization of the perovskite $LaYbO_3$, J. Phys. Conf. Series 687 (2016) 012104, , https://doi.org/10.1088/1742-6596/687/1/012104.
[48] Y. Obukuro, K. Ninomiya, M. Arai, Y. Okuyama, G. Sakai, S. Matsushima, First-principles study on $LaYbO_3$ as the localized f electrons containing system with MBJ–LDA + U approach, Comput. Mater. Sci. 126 (2017) 7–11, https://doi.org/10.1016/j.commatsci.2016.09.005.
[49] A. Løken, S. Ricote, S. Wachowski, Thermal and Chemical Expansion in Proton Ceramic Electrolytes and Compatible Electrodes, Crystals 8 (2018) 365, https://doi.org/10.3390/cryst8090365.
[50] R.D. Shannon, Revised effective ionic radii and systematic studies of interatomic distances in halides and chalcogenides, Acta Cryst. A32 (1976) 751–767, https://doi.org/10.1107/S0567739476001551.
[51] V. Kyriakou, I. Garagounis, A. Vourros, G.E. Marnellos, M. Stoukides, A protonic ceramic membrane reactor for the production of hydrogen from coal steam gasification, J. Membr. Sci. 553 (2018) 163–170, https://doi.org/10.1016/j.memsci.2018.02.047.
[52] A. Vourros, V. Kyriakou, I. Garagounis, E. Vasileiou, M. Stoukides, Chemical reactors with high temperature proton conductors as a main component: progress in the past decade, Solid State Ion. 306 (2017) 76–81, https://doi.org/10.1016/j.memsci.2018.02.047.
[53] N. Shi, Y. Xie, D. Huan, Y. Yang, S. Xue, Z. Qi, Y. Pan, R. Peng, C. Xiaa, Y. Lu, Controllable CO_2 conversion in high performance proton conducting solid oxide electrolysis cells and the possible mechanisms, J. Mater. Chem. A 7 (2019) 4855–4864, https://doi.org/10.1039/C8TA12458B.
[54] N. Danilov, A. Tarutin, J. Lyagaeva, G. Vdovina, D. Medvedev, CO_2-promoted hydrogen production in a protonic ceramic electrolysis cell, J. Mater. Chem. A 6 (2018) 16341–16346, https://doi.org/10.1039/C8TA05820B.
[55] A. Løken, T.S. Bjørheim, R. Haugsrud, The pivotal role of the dopant choice on the thermodynamics of hydration and associations in proton conducting $BaCe_{0.9}X_{0.1}O_{3-\delta}$ (X = Sc, Ga, Y, In, Gd and Er), J. Mater. Chem. A 3 (2015) 23289–23298, https://doi.org/10.1039/C5TA04932F.
[56] T. Tu, B. Zhang, J. Liu, K. Wu, K. Peng, Synthesis and conductivity behaviour of Mo-doped $La_2Ce_2O_7$ proton conductors, Electrochim. Acta 283 (2018) 1366–1374, https://doi.org/10.1016/j.electacta.2018.07.032.
[57] H. Yamamura, H. Nishino, K. Kakinuma, K. Nomura, Crystal phase and electrical conductivity in the pyrochlore-type composition systems, $Ln_2Ce_2O_7$ (Ln = La, Nd, Sm, Eu, Gd, Y and Yb), J. Ceram. Soc. Jpn. 111 (2003) 902–906, https://doi.org/10.2109/jcersj.111.902.
[58] M.J. Zayas-Rey, L. dos Santos-Gómez, D. Marrero-López, L. León-Reina, J. Canales-Vázquez, M.A.G. Aranda, E.R. Losilla, Structural and conducting features of niobium-doped lanthanum tungstate, $La_{27}(W_{1-x}Nb_x)_5O_{55.55-\delta}$, Chem. Mater. 253 (2013) 448–456, https://doi.org/10.1021/cm304067d.
[59] R. Haugsrud, C. Kjølseth, Effects of protons and acceptor substitution on the electrical conductivity of La_6WO_{12}, J. Phys. Chem. Solids 69 (2008) 1758–1765, https://doi.org/10.1016/j.jpcs.2008.01.002.
[60] M. Yuqing, G. Jun, Z. Zeyu, A. Jake, T. Jianhua, B. Kyle, Review: recent progress in low-temperature proton-conducting ceramics, J. Mater. Sci. 54 (2019) 9291–9312, https://doi.org/10.1007/s10853-019-03559-9.
[61] http://www.ihte.uran.ru/?page_id = 3142.